Chemical Engineering Science 176 (2018) 139–152

Contents lists available at ScienceDirect

Chemical Engineering Science

journal homepage: www.elsevier.com/locate/ces

Effect of surfactant on emulsification in microchannels

Nina M. Kovalchuk [a,*], Evangelia Roumpea [b], Emilia Nowak [a,1], Maxime Chinaud [b], Panagiota Angeli [b], Mark J.H. Simmons [a]

[a] School of Chemical Engineering, University of Birmingham, Edgbaston, Birmingham B15 2TT, UK
[b] Department of Chemical Engineering, University College London, Torrington Place, London WC1E 7JE, UK

HIGHLIGHTS

- Dynamic interfacial tension (DIT) is a key parameter for controlled drop production.
- Flow map is invariant in co-ordinates of capillary numbers based on DIT.
- Size of small drops increases as flow rate ratio to the power 0.1.
- Size of large drops increases as flow rate ratio to the power 1.
- Ionic surfactant can facilitate drop coalescence in microchannel.

GRAPHICAL ABSTRACT

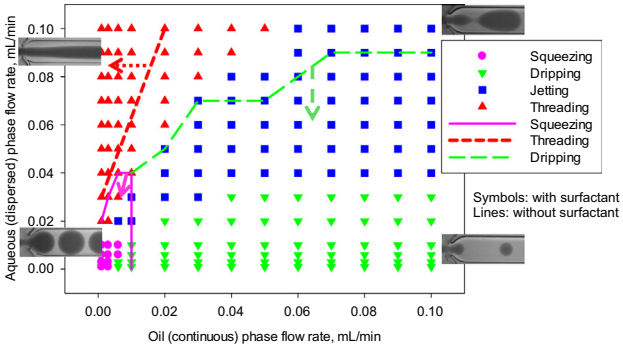

ARTICLE INFO

Article history:
Received 30 March 2017
Received in revised form 9 August 2017
Accepted 20 October 2017
Available online 21 October 2017

Keywords:
Microfluidic drop formation
Flow map
Ionic surfactant
Dynamic interfacial tension
Critical micelle concentration
Coalescence

ABSTRACT

Drop formation in a microfluidic flow-focusing device (cross-junction) was studied in absence and presence of one of two ionic surfactants. Four different flow regimes: squeezing, dripping, jetting, and threading were observed in line with existing literature. The effect of surfactant on the transition between flow regimes was shown to depend upon the value of critical micelle concentration and correlates with dynamic surface tension. Drop length in the channel increased as the ratio of flow rate of dispersed to continuous phase, φ, increased. For drops smaller than the channel width, the increase was slow, proportional to $\varphi^{0.1}$, yet was much faster, proportional to φ, for larger drops. In contradiction to the expected stabilisation of drops by surfactant, surfactant-laden drops larger than the channel height coalesced inside the channel at a higher rate than surfactant-free drops. It is proposed that the coalescence is caused by the electrostatic attraction due to surfactant redistribution under the high shear stresses near the wall of the channel.

1. Introduction

The behaviour of fluids within micro- and nano-devices is a rapidly growing scientific area due to numerous potential future applications in, for example, healthcare, molecular discovery and manufacture (Whitesides, 2006). One of the essential advantages of microfluidics is the capability for precise manipulation of multiphase flows, drops and bubbles to create bespoke products, in particular, using foaming and emulsification processes (Rodriquez- Rodriquez et al., 2015; Ushikubo et al., 2015; Vladisavljevic, 2016; Whitesides, 2006; Zhang et al., 2016) or arrays of droplets (Pompano et al., 2011). It also enables the study of interaction between drops, in particular, drop coalescence under conditions relevant to industrial emulsification processes (Baret et al.,

* Corresponding author.
E-mail address: n.kovalchuk@bham.ac.uk (N.M. Kovalchuk).
[1] Present address: Massey University, Auckland, 0745, New Zealand.

https://doi.org/10.1016/j.ces.2017.10.026
0009-2509/

2009; Bremond et al., 2008; Zhou et al., 2016). Comprehensive reviews covering various aspects of drop formation and manipulation in microfluidic devices can be found in Anna (2016); Baret (2012); Christopher and Anna (2007); Seemann et al. (2012).

Flow focusing is one of the most effective microfluidic methods for production of uniform drops. There are two versions of this method: geometrical flow focusing, where fluids are forced through an orifice with size smaller than the channel width (Anna et al., 2003; Garstecki et al., 2005; Lee et al., 2009) and hydrodynamic focusing, where the drop formation occurs in a cross-junction (Abate et al., 2009; Cubaud and Mason, 2008; Tan et al., 2008). Four different flow regimes can be identified within such flow focusing devices, namely squeezing, dripping, jetting and threading (Cubaud and Mason, 2008; Lee et al., 2009). At high viscosity ratio of two phases a fifth regime of tip streaming (Anna and Mayer, 2006; Ward et al., 2010), can be observed.

The large number of processes and physical parameters, and the interplay between them hampers development of predictive capability for the observed flow regimes. Many published studies have developed flow pattern transition criteria based upon a limited range of experimental parameters. As an example, the ratio of the viscosity between the dispersed phase, μ_d and the continuous phase, μ_c has been identified as a key parameter in many works (Anna and Mayer, 2006; Bai et al., 2016; Cubaud and Mason, 2008; Lee et al., 2009; Nie et al., 2008; Tan et al., 2008; Ward et al., 2010), yet the findings relating to other parameters are often dependent upon the type of experiment carried out. At high viscosity difference between the liquid phases (above 20 times) the occurrence of each regime seems to be determined by the flow rate of the more viscous phase, independent of the device geometry. In Cubaud and Mason (2008) transition from dripping to jetting/threading occurs by the increase of the flow rate of more viscous *dispersed* phase, Q_d, and the capillary number of dispersed phase at transition was found to be almost independent of the capillary number of continuous phase. However, in Anna and Mayer (2006); Lee et al. (2009) transitions were obtained by increasing the flow rate of the more viscous *continuous* phase, Q_c. When viscosity difference becomes less pronounced the situation becomes more complicated. At viscosity ratio $\mu_d/\mu_c = 1/6$, the transition from dripping to jetting was observed by increasing the flow rate of the *more viscous continuous* phase in Anna et al. (2003). However by using a different geometry at nearly the same $\mu_d/\mu_c = 3.4/19$ the transition from dripping to jetting to threading was observed by the increase of flow rate of *less viscous dispersed* phase (Humphry et al., 2009). Thus, there is a lack of a comprehensive study to unify these observations in terms of geometry and dimensionless parameters including flow rate, and viscosity ratio.

In the squeezing regime, sometimes referred to as a "geometry controlled regime" (Anna and Mayer, 2006; Bardin et al., 2013), a newly formed drop obstructs the channel or focusing orifice and restricts the flow of continuous phase. Consequently, the pressure inside the continuous phase increases (Romero and Abate, 2012) causing squeezing and pinch-off of a dispersed phase droplet (Lee et al., 2009). The size of the drop formed in squeezing mode is proportional to the channel width and flow rate ratio ($\varphi = Q_d/Q_c$) with coefficients depending on the geometrical parameters (Anna, 2016). Analysis of the pressure variations shows similarity in the drop formation mechanism in the squeezing mode in both a flow focusing geometry and in a T-junction (Romero and Abate, 2012).

An increase in the flow rate of the continuous phase (when $\mu_C > \mu_D$) results in the increase of viscous drag force applied to the dispersed phase. According to (Anna, 2016) the drop size formed in a T-junction then becomes dependent on the aforementioned viscosity ratio and the capillary number of the continuous phase. Due to similarities of squeezing regimes in the two microfluidic geometries the same can be expected for flow focusing devices. The evolving drop of dispersed phase becomes more and more elongated and at certain flow rate it ceases to obstruct channel. Then the dripping mode comes into play when the drop detachment is governed by viscous drag and capillary instability; this has been confirmed by numerical simulations (Zhou et al., 2006).

After the transition has been made from dripping to jetting, drops are formed at the end of an unstable jet well downstream of the focusing part of the geometry. From a fundamental perspective, this is generally associated with transition from absolute to convective instability (Guillot et al., 2009), although sometimes drop formation in the jetting regime can occur by absolute instability (Utada et al., 2008). Two different types of transition from dripping to jetting have been found in co-flowing geometries (Utada et al., 2007). The first is characterised by jet narrowing in the downstream direction and is caused by the viscous drag of the continuous phase exerted on the dispersed phase. In this case transition from dripping to jetting occurs by the increase of the flow rate of the continuous phase. For the second type of transition, jet thickness increases in the downstream direction. The driving force of this transition is not only the viscous drag, but also inertia of dispersed phase and this therefore occurs due to the increase of the flow rate of the dispersed phase.

These two types of dripping to jetting transitions give a possible explanation of the dependence of the transition from dripping to jetting on the flow rate of the more viscous phase. Transition caused by the viscous drag in the continuous phase is determined by the capillary number of continuous phase, i.e. the critical flow rate for this transition is inversely proportional to the viscosity of continuous phase. If the viscosity of continuous phase is sufficiently small, then transition due to the inertia of the dispersed phase occurs before the viscous effects come into play.

The occurrence of the final flow regime of interest to this study, threading, is due to further increases in either the flow rate of continuous or dispersed phase (depending on type of the transition from dripping to jetting). Threading occurs when the jet becomes stable and drops are no longer formed (Guillot et al., 2009; Humphry et al., 2009; Son et al., 2003). Such stable threads are impossible for unconfined flow, but geometrical confinement stabilizes the threads in microchannels with width larger than channel height. It has been shown in Son et al. (2003) that if a liquid thread becomes non-axisymmetric due to confinement, the minimum wavelength required to provide a decrease in surface area by deformation (i.e. the critical wave length for Rayleigh instability) increases with deviation of the thread aspect ratio of smaller to larger thread diameter from unity. At a certain thread aspect ratio the critical wavenumber becomes zero, i.e. the thread becomes absolutely stable because any deformation results in an increase of surface area (Guillot et al., 2009; Son et al., 2003). In Son et al. (2003) this prediction was confirmed for a system involving transport of two immiscible polymeric fluids, whereas in Humphry et al. (2009) it was confirmed for a microfluidic flow-focusing device.

According to (Humphry et al., 2009), an abrupt increase in the channel depth can further destabilise the thread and thus restart drop formation. The theoretical analysis performed in Humphry et al. (2009) predict that transition to threading regime occurs at

$$\frac{WQ_d\mu_d}{hQ_c\mu_c} > 1 \tag{1}$$

where W is the channel width, h is the channel height, Q is the flow rate, μ is dynamic viscosity and the subscripts d and c stand for dispersed and continuous phase respectively.

Regardless of the flow regime in which microfluidic device is working, an essential characteristic of a workable microfluidic

device is predictability of drop size and frequency (formation time), as well as maintaining a narrow or ultimately unimodal drop size distribution. Despite considerable progress made over the last decade with several models proposed to relate the drop size to device operational parameters including properties of liquids (Chen et al., 2015; Cubaud and Mason, 2008; Lee et al., 2009; Liu and Zhang, 2011) and predict transitions of dynamic regimes (Humphry et al., 2009; Liu and Zhang, 2011; Son et al., 2003; Zhou et al., 2006) it is still impossible to predict performance of a particular device with the necessary reliability. As already stated, the reason is that the drop properties are determined by a very large number of parameters, such as method of focusing (geometrical, hydrodynamic or combined), device geometry, viscosities of liquids involved and flow rates. The situation is complicated even further if surfactant(s) are present, whose influence will depend upon their concentration and type. Therefore more experimental studies are needed to choose between existing models and provide data for validation of new more general models.

The purpose of surfactant addition is to stabilise produced droplets (or bubbles) against coalescence. Besides stabilisation, the presence of surfactant affects the process of drop formation through modification of capillary forces and interfacial viscoelasticity. Thus the understanding of the effect of surfactant on the performance of microfluidic emulsification/foaming devices, in particular in terms of drop size and size distribution is of great practical importance.

Given that the characteristic time of drop formation in microfluidic devices is in the sub-second range, it is clear that the dynamic interfacial tension on the corresponding time scale rather than equilibrium values should be taken into account. Therefore, studies on formation of surfactant-laden drops/bubbles in microfluidic devices are also contributing to the solution of a fundamental problem of short time surfactant dynamics and mass transfer in liquid/liquid systems. The importance of dynamic interfacial tension for the performance of microfluidic device is stressed in many publications (Chen et al., 2015; Glawdel and Ren, 2012; Roche et al., 2009; Wang et al., 2016). In particular, it was shown that microfluidics is a promising tool for measurement of dynamic interfacial tension on short time scales up to the sub-millisecond range (Brosseau et al., 2014; Muijlwijk et al., 2016; Steegmans et al., 2009; Wang et al., 2009).

Recent studies have shown that even if surfactant is present in microfluidic systems in high concentrations, the effect of dynamic interfacial tension can be considerable. It was found for example in Wang et al. (2009) that the size of droplets formed in T-junction depended on the concentration of Tween 20 surfactant even at concentrations 300 times higher than critical micelle concentration (*CMC*). At the same time no effect of concentration on the drop size was found in this study for another surfactant, sodium dodecyl sulphate, at concentrations 2CMC and higher. This example shows that the effect of a surfactant depends not only on surfactant concentration, but also on its other properties. (Glawdel and Ren, 2012), who examined droplet formation in T-junction in the squeezing-to-transition regime (Glawdel et al., 2012), proposed the following expression for the deviation of dynamic surface tension from its equilibrium value

$$\Delta\gamma(t) = \frac{nRT\Gamma_{CMC}^2}{CMC}\sqrt{\frac{3\pi}{4D_{eff}}}\sqrt{\frac{f_3^2 t}{(f_3 t)^2 + 3f_3 t + 3}} \tag{2}$$

where t is the time, $n = 1$ for non-ionic surfactants and $n = 2$ for ionic surfactants, R is the gas constant, T is the absolute temperature, *CMC* is the critical micelle concentration, Γ_{CMC} is the surface coverage at *CMC*, $D_{eff} = D(1+\beta)(1+\beta\sigma^2)$ is the effective diffusion coefficient taking into account contribution of micelles to the transport of surfactant, D is the diffusion coefficient of monomers, $\beta = \frac{c_0}{CMC} - 1$, c_0 is the initial surfactant concentration, $\sigma^2 = N_a^{-1/3}$, N_a is the number of monomers per micelle (aggregation number), $f_3 = \frac{2Q_d}{w_d h^2}[1 + (h/w_d)^{1/2}]$, Q_d is the flow rate of dispersed phase, w_d is the width of the channel for the dispersed phase, h is the channel height.

The above model is based on the approach developed by Joos (Joos and Van Uffelen, 1995; Joos, 1999) for calculation of interfacial tension on a continuously deformed interface in presence of micelles. Note that Eq. (2) gives the effective value of interfacial tension, whereas the real interfacial tension can be non-uniform in space. In particular, non-uniform distribution of surfactant can result in surfactant-mediated tip streaming in microfluidic flow focusing devices (Anna and Mayer, 2006; Anna, 2016; Ward et al., 2010).

Eq. (2) shows that the deviation of interfacial tension from the equilibrium value decreases with an increase of characteristic time of drop formation, surfactant diffusion coefficient, concentration (through D_{eff}) and the value of *CMC*, whereas it increases with the square of Γ_{CMC}. It appears that the dependence on Γ_{CMC} is stronger than on *CMC*, but one should take into account that Γ_{CMC} is of the same order of magnitude for the most surfactants, whereas *CMC* can differ in several orders of magnitude. Therefore it can be concluded from Eq. (2) that *CMC* is the most important parameter determining the effect of surfactants on the performance of a microfluidic device. Although Eq. (2) is derived for T-junction and time dependence of deviation from the equilibrium interfacial tension is specific to this type of device, the prefactor, i.e. the dependence on surfactant characteristics is device-independent. A study performed on formation of surfactant laden drops of microlitre size without geometrical confinement (Kovalchuk et al., 2016) has confirmed importance of surfactant *CMC* for this process.

Despite the obvious importance of *CMC* there is no systematic study of the effect of this parameter on the performance of a microfluidic device. Moreover, there is no systematic data on the effect of surfactant upon the occurrence of each flow regime as shown in a flow map. Flow maps for the surfactant-laden and surfactant-free continuous phase were compared in Van Loo et al. (2016), but only one concentration of surfactant was studied. A very high surfactant concentration was used in Van Loo et al. (2016), so the dynamic effects related to surfactant adsorption were not considered.

To fill the existing gaps identified above, this paper presents a comprehensive study on the effect of surfactant on flow regime transition in flow-focusing microfluidic device. To study the effect of *CMC*, two surfactants belonging to the same family, alkyltrimethylammonium bromides, but with different alkyl chain length were used. The difference in the values of *CMC* for these surfactants is about one order of magnitude. The surfactant solutions chosen have very close values of equilibrium surface tension at *CMC*, Γ_{cmc} and monomer diffusion coefficients. Likewise, the chosen values c_0/CMC are very close for both surfactants, therefore the values of the effective diffusion coefficients are also close to each other. Under such conditions it is possible to independently follow the effect of *CMC* and concentration upon performance of the microfluidic device.

The paper is structured as follows; Section 2 describes the experimental methods, including the choice of fluids and surfactants, measurement of fluid physical properties and choice of microfluidic chip. The obtained results are discussed in Section 3. The results of the equilibrium interfacial tension and dynamic surface tension measurements for the surfactant-laden fluids are described in Section 3.1, which sets the context for the expected behaviour of the fluids with respect to observed flow regime tran-

sitions, which is covered in Section 3.2. Section 3.3 focuses on the shape of the drops and their size distribution as a function of flow regime and flow conditions whilst Section 3.4 describes the effect of surfactant on drop coalescence phenomena observed downstream from the region of drop formation. The conclusions from the study are presented in Section 4.

2. Experimental methods

The surfactants, dodecyltrimethylammonium bromide (C_{12}TAB), Across organics, 99% and hexadecyltrimethylammonium bromide (C_{16}TAB), Sigma, BioXtra, ≥99%; glycerol, Sigma, for molecular biology, ≥99%; and silicone oil, viscosity standard 5 cSt, Aldrich were used without additional purification. Double-distilled water was produced by Aquatron A 4000 D, Stuart.

Silicone oil was used as a continuous phase, whereas 52% water/48% glycerol mixture (w/w) was used as the dispersed phase. The surfactant was dissolved in the aqueous (dispersed) phase. Both surfactants used are insoluble in the oil (continuous) phase. To enhance optical contrast, Parker black ink or methyl violet dye were added to the aqueous phase. The ink or dye addition does not change the interfacial tension between the oil and aqueous phase above the level of experimental error.

Experiments were performed using a Droplet Junction Chip (cross-junction) made of glass with hydrophobised channels (Dolomite Microfluidics, UK). The geometry as presented in Dolomite Product Datasheet is shown in Fig. 1. The geometry of chip combines both hydrodynamic and geometrical flow focusing. Note, most experiments on drop formation in microfluidic flow focusing devices are performed in channels having rectangular cross-section (Anna, 2016), as such devices are easily fabricated using soft lithography. The characteristic feature of such devices is that it is possible for the continuous phase to flow along the corners of the geometry even if the dispersed phase forms plugs with a width close to the channel cross-section. There are no corner gutters in the geometry presented in Fig. 1 (the corners are rounded), therefore the use of this geometry allowed understanding of the possible effect of gutters on drop formation.

The liquids were supplied to the chip using syringe pumps Al-4000 (World Precision Instruments, UK), equipped with 10 mL syringes (BD Plastipak™) at flow rates, Q, in the range of 0.001–0.1 mL/min. After any change in flow rate the system was allowed to stabilize for at least 10 min. The flow regimes and formed structures were monitored at 2000 fps using a high speed videocamera (Photron SA5) equipped with a Navitar, 2X F-mount objective. Image processing was performed using ImageJ free software. The presented values of drop size and frequency are an average from 30 drops measured. The experimental error did not exceed 3% for drops with size smaller than the channel width and was within 30% for larger drops. Small experimental error for drop size (small drops) and similar error for distances between drops confirm that the pulsating of the flow created by syringe pumps does not affect the experimental results.

The equilibrium interfacial tension was measured using a tensiometer K100 (Krüss) equipped with a Du Noüy platinum ring. The dynamic surface tension was measured using a maximum bubble pressure tensiometer BPA-1S (Sinterface, Germany).

The viscosity was measured by a TA instruments Discovery-HR-2 rheometer in flow mode using cone and plate geometry with the angle 2° 0′ 29″ and a truncation of 55 μm.

According to the complicated chip geometry flow focusing in the cross-junction occurs through two mechanisms complementing each other: hydrodynamic flow focusing due to liquid flows coming together in the X-junction (Cubaud and Mason, 2008; Lee et al., 2009) and geometrical focusing due to the decrease of channel cross-section at the junction (Anna et al., 2003; Garstecki et al., 2005). It is therefore, complicated to choose the parameters included in the dimensionless numbers for flow characterisation. As the varied parameters in this study are the liquid flow rates directly related to the hydrodynamic focusing, the flow parameters in the feeding channels (wide channels in Fig. 1) are used for flow characterisation. The hydraulic radius (R_c = 67 μm) corresponding to the wide channel cross-section, S, is chosen as a characteristic length scale. Note, the flow rates (Q_d for dispersed phase and Q_c for continuous phase) in what follows are ascribed for the feeding channels and thus the oil flow rate in the output channel is $2{\cdot}Q_c$. The physical properties of the liquids used in this study are presented in Table 1.

3. Results and discussion

3.1. Interfacial/surface tension

Interfacial tension isotherms for surfactants in the glycerol/water mixture with silicone oil are presented in Fig. 2. As can be seen, the *CMC* values, ~2 mM for C_{16}TAB and ~20 mM for C_{12}TAB, are larger when compared with solutions in pure water (~0.9 mM for C_{16}TAB and ~15 mM for C_{12}TAB (Kovalchuk et al., 2016)). Interfacial tensions at concentrations above *CMC* are close to each other for both, being 7.3 mN/m for C_{16}TAB and 10 mN/m for C_{12}TAB.

These results enable the choice of two concentrations of each surfactant for this study. Smaller concentrations (c_0 = 0.35 mM for C_{16}TAB and c_0 = 5 mM for C_{12}TAB) are below *CMC*, and correspond to the same equilibrium interfacial tension of 20 mN/m. Larger concentrations (c = 5 mM for C_{16}TAB and c = 50 mM for C_{12}TAB) are around 2.5 times of *CMC* for each surfactant giving a similar micellar contribution to the effective diffusion coefficient in Eq (2). Additionally a concentration of 150 mM was studied for C_{12}TAB.

The reliable measurement of dynamic interfacial tension on the timescale of interest is a challenging problem, not quite solved yet; therefore the dynamic surface tension (aqueous solution/air interface) for the studied solutions is presented in Fig. 3. Despite the difference in the adsorption kinetics to aqueous solution/air and aqueous solution/oil interface caused by the difference in adsorption isotherms, the data of Fig. 3 provide a guideline for dynamic interfacial tension, especially taking into account that diffusion coefficients are independent of the second phase. The surface tension of 52% glycerol/48% water mixture is around 66 mN/m, whereas the equilibrium surface tension of 0.35 mM C_{16}TAB and 5 mM C_{12}TAB is about 50 mN/m. The equilibrium surface tension of solutions of both surfactants above *CMC* is about 37 mN/m.

Fig. 3 shows that the kinetics of surfactant equilibration besides concentration depends on the *CMC* value. If we compare results for the two surfactants with concentrations 2.5 times higher than CMC (C_{16}TAB 5 mM and C_{12}TAB 50 mM), it is obvious that surfactant with higher CMC equilibrates much more quickly. In particular, the surfactant with higher CMC value has the surface tension close to the equilibrium value at a time equal to 0.01 s, whereas for surfactant with 1 order of magnitude lower CMC the surface tension at 0.01 s is close to the surface tension of aqueous phase without surfactant. This result is in line with Eq. (2) and shows that adding surfactant even at concentrations several times higher than the CMC does not guarantee that the system operates at equilibrium surface tension on the time scale of drop formation in microfluidic device if CMC value is small. It should be reminded that the difference in the equilibration rate shown in Fig. 3 is mostly due to the difference in the CMC values, because the diffusion coefficients for two surfactant monomers are quite close to each other: $8{\cdot}10^{-11}$ m^2/s for C_{16}TAB and $9{\cdot}10^{-11}$ m^2/s for C_{12}TAB as estimated using Wilke-Chang correlation (Wilke and Chang, 1955). The effective

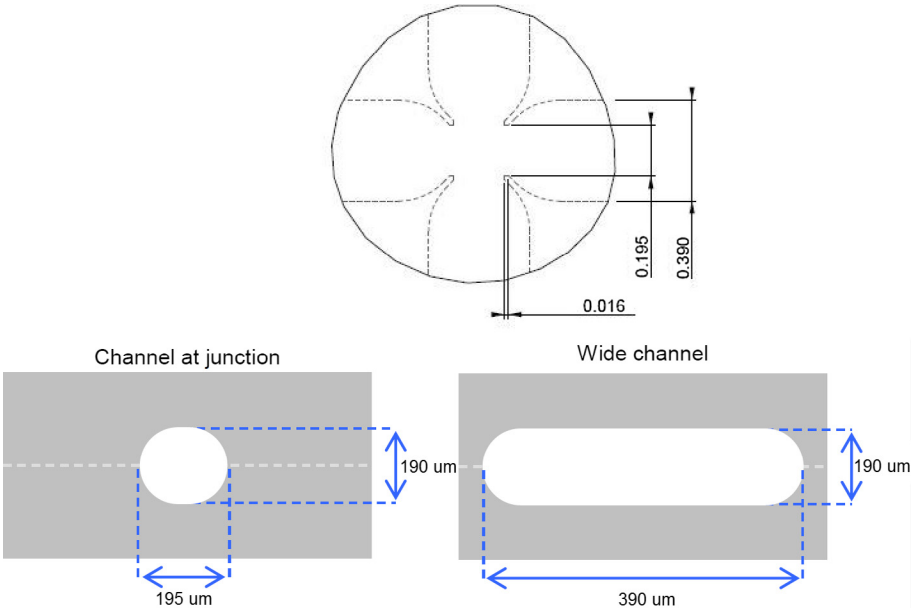

Fig. 1. Microfluidic chip geometry. Adapted with permission from the Dolomite Product Datasheet.

Table 1
Physical properties of the liquid phases.

Liquid	Density, kg/m3	Dynamic viscosity, mPa s	Interfacial tension, mN/m
Water/glycerol mixture 52:48 (w:w), dispersed phase	1133	6	29
Silicone oil, continuous phase	920	4.6	

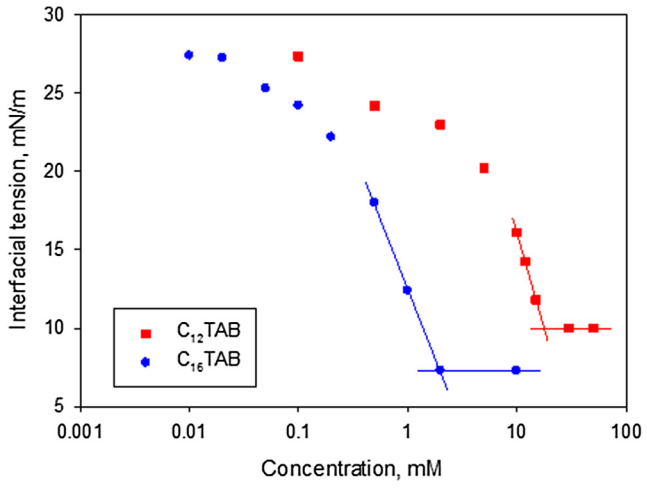

Fig. 2. Interfacial tension isotherms for C_{12}TAB and C_{16}TAB at aqueous/oil interface.

diffusion coefficients taking into account the micellar contribution to diffusion are also very close to both surfactants because of the similar values of c_0/CMC = 2.5.

Given that the time scale of interest for this study is 0.005 s < t<0.5 s, the effect of dynamic interfacial tension on this timescale is expected as follows.

- The dynamic surface tension of 0.35 mM C_{16}TAB (~0.2 *CMC*) is close to that glycerol/water mixture without surfactant. It is therefore expected that this solution should behave like surfactant-free in microfluidic drop formation.

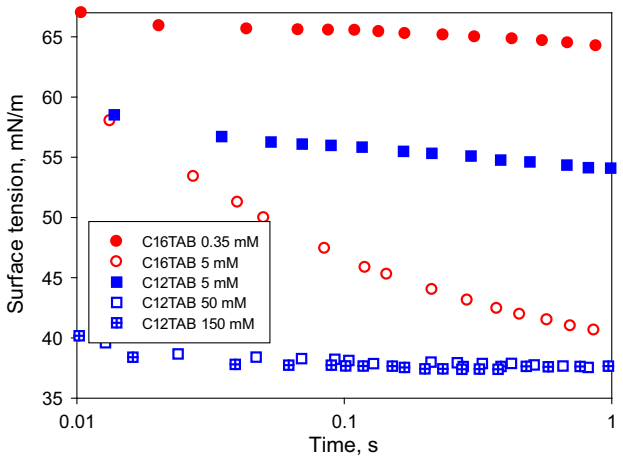

Fig. 3. Dynamics surface tension of C_{16}TAB and C_{12}TAB at concentrations used in this study. Filled symbols correspond to concentrations below CMC, crossed and empty symbols correspond to concentrations above CMC.

- The dynamic surface tension of 5 mM of C_{12}TAB (0.25 *CMC*) is quite close to the equilibrium value except for the shortest times of several milliseconds; therefore this surfactant should behave differently from the former one despite the similar equilibrium interfacial tension.
- Both 50 and 150 mM C_{12}TAB solutions (2.5 and 7.5 *CMC* correspondingly) are at thermodynamic equilibrium on the timescale of interest, therefore their behaviour should be similar to each other, but different from that of 5 mM C_{12}TAB because of difference in equilibrium interfacial tension.
- The dynamic surface tension of 5 mM solution of C_{16}TAB (2.5 *CMC*) is close to 5 mM C_{12}TAB on the time scale of millisecond and close to 50 mM C_{12}TAB on the time scale of hundreds of milliseconds. Therefore its behaviour i.e. mechanism of formation, drop size and frequency should be close to that of 5 mM C_{12}TAB at high flow rates, but it should be close to that of 50 mM C_{12}TAB at low flow rates.

This analysis is in line with Eq. (2) which predicts considerable difference in the behaviour for surfactants with different *CMC* values. In the below, the assumptions made above will be tested against the performance of these solutions during drop formation in the microfluidic device. Note, the data for 150 mM of C_{12}TAB solutions are not presented in the following graphs, because they were found to be practically similar to those of 50 mM solution, confirming that in the range of flow rates considered here both solutions have the same value of dynamic interfacial tension close to the equilibrium one.

There are two possible approaches in consideration of the performance of the microfluidic device. One is based on consideration of flow regimes and another is based on drop sizes and shapes. These approaches do not coincide, except for a thread, as a drop of the same shape can be produced in different regimes, for example, plug can be formed by squeezing or by jetting.

3.2. Flow regime transitions

Let us first consider the effect of surfactant on flow regime transitions. Considering both fluids have similar values of kinematic viscosity $\nu = \mu/\rho$, where μ is dynamic viscosity and ρ is density, the Reynolds number, $Re = QR_c/S\nu$, based on the flow rates in the feeding channels is in the same range for both liquids: $0.003 < Re < 0.3$. As $Re < 1$ in the whole range of the flow rates studied, the inertial effects are less important than the viscous ones and therefore capillary numbers, $Ca = \mu Q/S\gamma$, where γ is the interfacial tension were chosen for characterisation of flows of both the dispersed and continuous phases. For liquids without surfactant the values of capillary number in each, dispersed and continuous phase, are in the range $5{\cdot}10^{-5} < Ca < 5{\cdot}10^{-3}$. The small values of capillary number imply that the interfacial tension determines to the large extent the system behaviour. The presence of surfactant decreases the interfacial tension and increases the value of capillary number, making therefore viscous effects more important. It is however not straightforward to determine the values of capillary number for surfactant solutions in the highly dynamic processes considered here, because the values of effective dynamic interfacial tension acting at the timescale of drop formation and detachment are unknown and can be very different from the equilibrium values. Therefore, in what follows, the flow maps for pure liquids and surfactant solutions will be shown in the co-ordinates of flow rates.

Typical images for each regime are shown in Fig. 4. The flow map for surfactant free system is presented in Fig. 5a and the flow map for aqueous phase containing 50 mM C_{12}TAB in Fig. 5b. Comparison of the flow maps shows clearly that the presence of surfactant moves transition to jetting and threading to smaller flow rates of the dispersed phase and the transition from squeezing to smaller flow rates of continuous and dispersed phase. According to Fig. 3 surfactant-laden system with 50 mM C_{12}TAB should have equilibrium interfacial tension on the time scale of drop formation in the whole range of flow rates. Therefore for this particular system comparison of the flow maps can be done also in terms of capillary number (see the areas outlined in Fig. 5), displaying close similarity of two systems.

The flow map for 0.35 mM (0.18 *CMC*) C_{16}TAB is similar to that of the system without surfactant. The flow maps for 5 mM (0.25 *CMC*) C_{12}TAB and 5 mM (2.5 *CMC*) C_{16}TAB are intermediate between those shown in Fig. 5a and b, with map for 5 mM (2.5 CMC) of C_{16}TAB coinciding with that of 50 mM (2.5 CMC) of C_{12}TAB at flow rates $\leq$0.04 mL/min (see Fig. 7 for dripping to jetting transition).

It was observed that at small flow rate of continuous phase the drops are formed in squeezing regime (Figs. 4-1, 5): the growing drop obstructs the channel cross-section at junction and the neck thinning and drop detachment occurs mainly under the rising pressure of continuous phase upstream of the junction (Anna, 2016; Anna and Mayer, 2006; Bardin et al., 2013; Lee et al., 2009; Romero and Abate, 2012). The transition from squeezing to the dripping mode is determined by the flow rate of continuous phase, in good agreement with the literature data (Anna, 2016; Anna and Mayer, 2006). Surfactant addition decreases the flow rate of continuous phase, but the capillary number of transition remains nearly the same ($Ca \sim 0.001$).

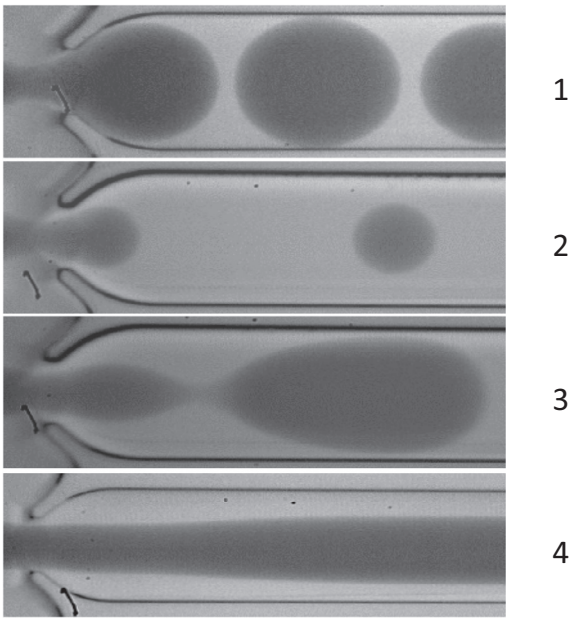

Fig. 4. Dynamic regimes in flow focusing device (surfactant-free system): 1 – squeezing, Q_c = 0.003 mL/min, Q_d = 0.01 mL/min; 2 – dripping, Q_c = 0.04 mL/min, Q_d = 0.01 mL/min; 3 – jetting, Q_c = 0.04 mL/min, Q_d = 0.1 mL/min; 4 – threading, Q_c = 0.01 mL/min, Q_d = 0.07 mL/min.

According to (Anna, 2016) squeezing regime is expected at $Ca_c < 0.01$. In our study squeezing regime was observed at $Ca_c < 0.001$ what is in line with the results of (Anna, 2016). However in Lee et al. (2009) it was observed at $0.1 < Ca_c < 1$. The difference in the threshold values of capillary number can be due to an additional effect of hydrodynamic flow focusing, difference in the channel geometry, flow rates and viscosity ratios. The importance of the last parameter for performance of microfluidic device was stressed, for example, in Bai et al. (2016); Nie et al. (2008). The difference in the geometry between our study and that of (Lee et al., 2009) is also considerable, as in Lee et al. (2009) geometrical flow focusing was used with the size of orifice much smaller than the size of channel, i.e. in their case the forming drop obstructed the orifice, but not the cannel. In our study, due the shape of channel at cross-junction, the drop obstructed both the focusing part and the channel. Another source of discrepancy in the results can be the criteria used to determine the regime transition. The transition between squeezing and dripping regime in our study was found from the image analysis: dripping was identified when the noticeable gap was observed between the drop surface and the channel wall. The error of this method is of order of the step in the capillary number.

In the dripping regime (Figs. 4-2, 5) there is no complete obstruction of flow by the growing drop and viscous effects become more important (Anna, 2016). The increase of the flow rate of dispersed phase by keeping constant the flow rate of continuous phase moves the pinch-off point downstream, which results in the transition from dripping to the unstable jet regime (Figs. 4-3, 5).

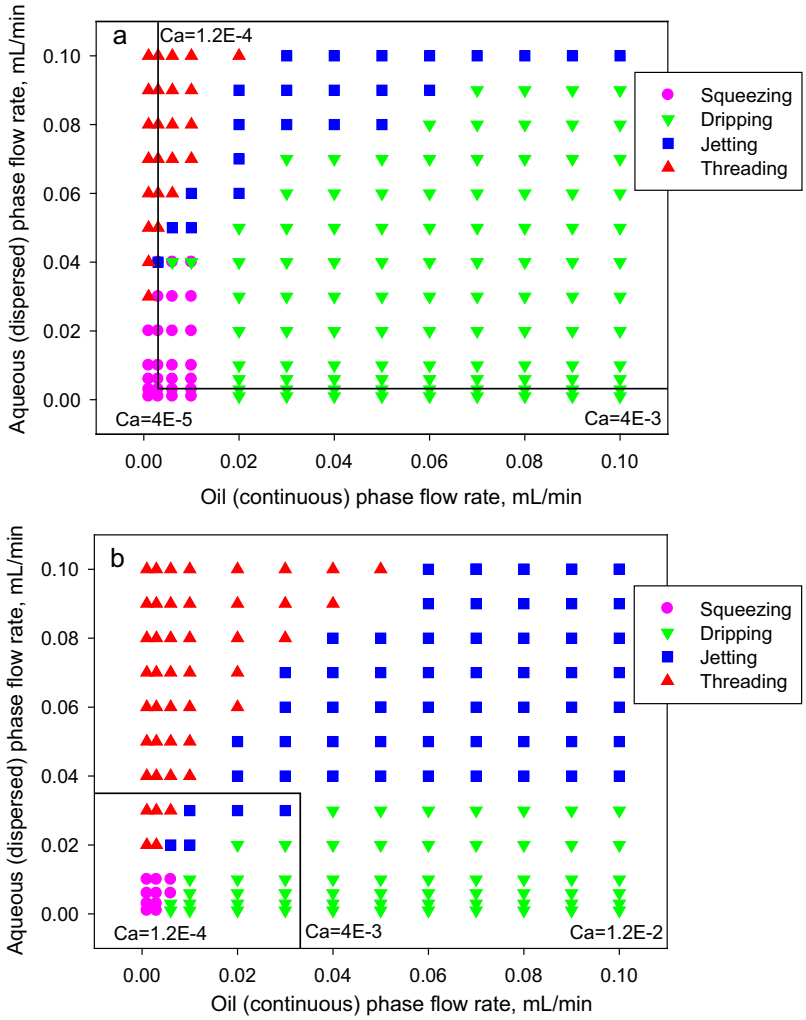

Fig. 5. Flow maps for regime transitions: a – no surfactant in dispersed phase, b – 50 mM C_{12}TAB in dispersed phase. The lines circumscribe the coinciding areas in the terms of capillary number for surfactant-free and surfactant-laden system. The first (from the left) value of the capillary number correspond to the minimum flow rate used (0.001 mL/min), the second one correspond to the line and the third one correspond to the maximum flow rate used (0.1 mL/min).

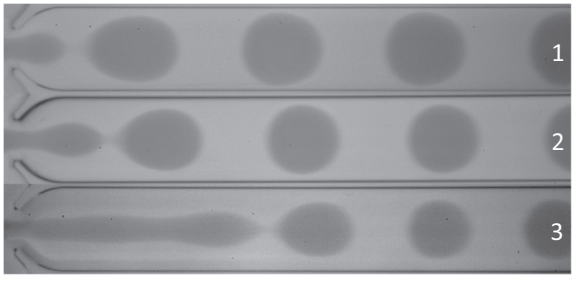

Fig. 6. Dependence of distance to the pinch-off point on surfactant concentration: 1 – surfactant-free aqueous solution, 2 – 5 mM of C_{12}TAB, 3 – 50 mM of C_{12}TAB. $Q_c = Q_d = 0.1$ mL/min.

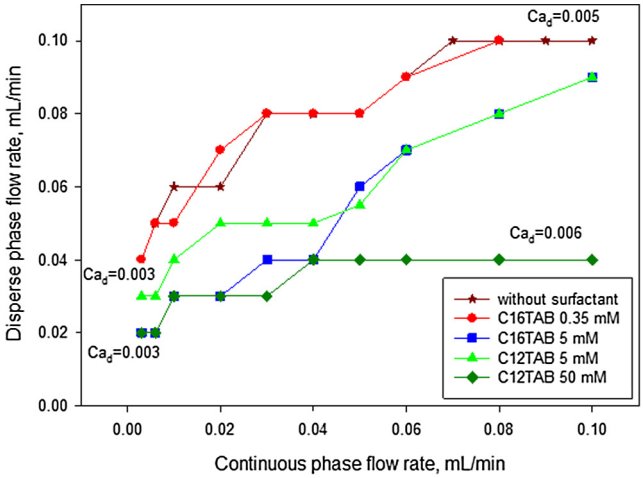

Fig. 7. Transition from dripping to jetting. Values of Ca_d are given for the first and the last point on the curves for pure water and solution of C_{12}TAB 50 mM.

The difference between dripping and jetting regime is visually obvious in most cases, because in the jetting regime there is always at least one varicose deformation between the junction and the pinch-off point (sf. Figs. 4-1, 2 and Fig. 4-3). As a complementary criterion, the one proposed in Cubaud and Mason (2008); Utada et al. (2007) was used: dripping corresponds to the case when the cap formed by the dispersed phase remains inside the junction after pinch-off. The distance from the end of junction to pinch-off point increases with the increase of the flow rate ratio in jetting regime, but for the system without surfactant it does not exceed 500 μm ($Q_c = 0.02$, $Q_d = 0.09$ mL/min). The critical length of jet (before pinch off) should be proportional to the visco-capillary

time scale $t_{cap} = \frac{R_c \mu}{\gamma}$ (Cubaud and Mason, 2008), i.e. inversely proportional to the interfacial tension. The increase of jet length with the decrease of interfacial tension is confirmed by Fig. 6.

At high viscosity difference, transition from dripping to jetting in flow focusing devices is determined mainly by the capillary number of the more viscous liquid and is practically independent of the flow rate of less viscous liquid (Anna and Mayer, 2006; Cubaud and Mason, 2008; Lee et al., 2009). As viscosities of dispersed and continuous phases are close to each other in this study, the critical capillary number for the transition depends considerably on both flow rates (see Fig. 7). Transition from dripping to jetting was observed with increasing flow rate of the dispersed phase, and the jet is widening downstream the junction (Figs. 4-3, 6). Therefore according to (Utada et al., 2007) inertia of dispersed phase should be of importance for this transition. However comparison of capillary and Weber ($We = \frac{\rho Q^2 R_c}{S^2 \gamma}$) numbers at transition between surfactant-free system and surfactant-laden systems close to equilibrium on the timescale of drop formation (50 and 150 mM of C_{12}TAB) shows that transition occurs at the similar values of capillary numbers (Fig. 7), whereas Weber numbers at the transition are considerably different. Therefore it can be concluded that transition is governed by capillary number rather than by the Weber number (Fig. 7), i.e. viscosity of inner phase is important for this transition.

It is obvious from Fig. 7 that the critical flow rate of dispersed phase for transition from dripping to jetting at given flow rate of continuous phase decreases with addition of surfactant. The effect of surfactant depends on its concentration and CMC and is in complete agreement with analysis based on dynamic surface tension. The transition occurs at similar flow rates for solution of 0.35 mM of C_{16}TAB and surfactant-free aqueous phase. The transition flow rate ratio decreases for 5 mM of C_{12}TAB and further decreases for 50 mM of C_{12}TAB. Transition for 5 mM of C_{16}TAB occurs at the same Q_d as for 50 mM of C_{12}TAB at low flow rates ($\leq$0.04 mL/min) and at the same Q_d as for 5 mM of C_{12}TAB at high flow rates (sf with dynamic surface tension isotherm in Fig. 3). Thus, results presented in Fig. 7 confirm the importance of CMC value for performance of a microfluidic device containing surfactant.

As it is seen from dynamic surface tension (Fig. 3) and from comparison of results for solutions of C_{12}TAB at concentrations 50 mM and 150 mM, solution of 50 mM C_{12}TAB behaves like a pure liquid with the interfacial tension close to the equilibrium value (10 mM/m) at all flow rates under study. The small deviations from equilibrium can be expected only at the highest flow rates used. Therefore the capillary numbers at dripping to jetting transition for this surfactant solution can be calculated using the value of equilibrium interfacial tension. Results presented in Fig. 7 demonstrate that transitions occur at similar values of capillary numbers for surfactant-free system and 50 mM solution of C_{12}TAB. A slightly larger value at high flow rates can be due to incomplete equilibration of surfactant on shorter time scales or just because of too large a step in flow rate. Assuming that transition from dripping to jetting at a certain flow rate of continuous phase occurs at the same value of capillary number for all dispersed phases used, it is possible to calculate the effective value of dynamic interfacial tension at transition, γ_{SL}, as

$$\gamma_{SL} = \gamma_{SF} \frac{\mu_{SL} Q_{SL}}{\mu_{SF} Q_{SF}} \quad (3)$$

where, γ_{SL}, μ_{SL} and Q_{SL} are correspondingly the interfacial tension, viscosity and flow rate for surfactant-laden aqueous phase, whereas μ_{SF} and Q_{SF} are viscosity and flow rate for surfactant-free aqueous phase. Corresponding values of the effective interfacial tension for 5 mM solution of C_{16}TAB are presented vs characteristic time of drop formed in jetting regime at transition by symbols in Fig. 8. The line in Fig. 8 is obtained by mapping the values of corresponding dynamic surface tension from Fig. 3 into interfacial tension. To do that the maximum surface pressure, i.e. the maximum difference in the equilibrium interfacial tension between surfactant-free and surfactant-laden (C_{16}TAB) system was compared for aqueous/air and aqueous/oil interfaces. Corresponding values are for aqueous/air interface $\Pi_{max,\ air} = 66–37 = 29$ mN/m, whereas $\Pi_{max,\ oil} = 29–7.3 = 21.7$ mN/m. Therefore scaling factor $F = \Pi_{max,\ oil}/\Pi_{max,\ air} = 0.748$. Thus, if at certain time of drop formation dynamic surface pressure for aqueous/air interface (found from Fig. 3) is $\Pi_{d,\ air}$, it can be assumed that the dynamic surface pressure for aqueous/oil interface is $\Pi_{d,\ oil} = F \cdot \Pi_{d,\ air}$. Of course, this is a very rough approximation, but Fig. 8 demonstrates a reasonably good agreement of two sets of data confirming that the dynamic surface tension can be used for the estimation of dynamic interfacial tension at the time scale of interest. Considering that Eq. (3) is based only on assumption of the same capillary number at transition and does not include for example, any model for the size of drops formed, it can be a good basis for the estimation of dynamic surface tension at liquid/liquid interface in the millisecond time range.

Further increase of the flow rate of dispersed phase results in transition to threading regime, which corresponds to the stable thread being observed over a distance at least $20R_c$ (where R_c is the hydraulic radius of channel) from the junction (Fig. 4-4). Note, for the system without surfactant the transition from the unstable jet to thread is well defined, because it corresponds to an abrupt increase of the jet length from 500 μm to > 4000 μm. For surfactant solutions the critical length of jet before transition to threading increases when compared to the surfactant-free system (see Fig. 5), but still the transition is well defined in the studied range of flow rates. The observed thread must be stable over the whole length of downstream channel due to geometrical confinement for the case when the thread width is comparable to or larger than the channel height (Humphry et al., 2009; Son et al., 2003). In our study the thread width increases with the increase of flow rate ratio $\varphi = Q_d/Q_c$ and is always larger than the channel height (190 μm). Substituting data for the channel geometry and viscosities into Eq. (1) one obtains that the threads in the system considered here should be stable at $Q_d/Q_c > 0.4$. The minimum value of Q_d/Q_c for threading in this study is 4, thus confirming that the observed threads are stable.

According to (Cubaud and Mason, 2008) transition from dripping to jetting/threading occurred in devices with hydrodynamic flow focusing at $Ca_d \sim 0.1$. In our study transition occurs over a range of $5 \cdot 10^{-3} < Ca_d < 4 \cdot 10^{-3}$ depending on flow rate ratio. The values of Ca_d investigated in Cubaud and Mason (2008) are higher than those in the present study, but the values of Ca_c cover the range of this study $5 \cdot 10^{-5} < Ca_c < 5 \cdot 10^{-3}$. Some discrepancy here can be due to the choice of flow velocities in channel for calculation of capillary number. As geometry in our study includes geometrical focusing, whereas that in Cubaud and Mason (2008) does not, probably for comparison we need to redefine capillary number using the liquid velocity in the focusing part. In this case capillary number in our study should be increased by factor 2.26, but still the difference with (Cubaud and Mason, 2008) is one order of magnitude. Another reason could be due to difference in the channel shape, in particular the presence the gutter flows in the corners of rectangular channels used in Cubaud and Mason (2008). It can be assumed that the preferable flow of the continuous phase through the corner gutters results in thinner films between the channel walls and drop surface and that this confinement stabilises the dripping regime. However, more probably from our point of view this is due to the effect of very different viscosity ratios (Nie et al., 2008). Another difference of results of our study from those reported in Cubaud and Mason (2008) is the dependence of the thread width on flow rate ratio. According to (Cubaud and

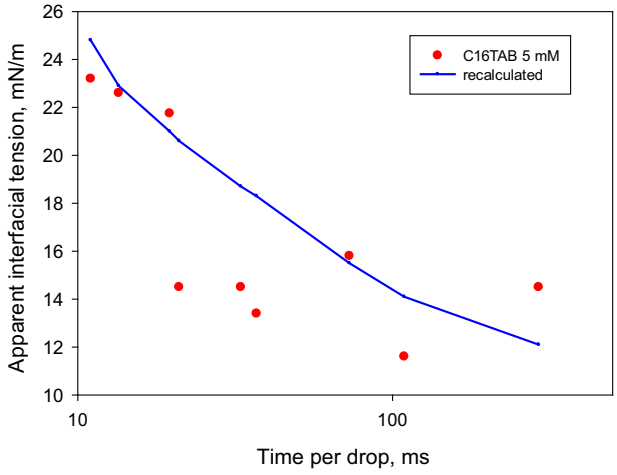

Fig. 8. Dynamic interfacial tension of 5 mM solution of $C_{16}TAB$ at dripping to jetting transition. The points are obtained from Eq. (3). The line is obtained by mapping data for dynamic surface tension, see text for details.

Mason, 2008) the thread width is proportional to $\varphi^{0.5}$, whereas in the present study a power law exponent, β, was found to be β = 0.22 ± 0.03. The effect of surfactant on transition flow rate ratio is similar to that discussed above for dripping to jetting transition.

3.3. Drop size and shape

As drop size and size distribution are of great practical interest, the effects of surfactants on the drop size and shape are considered further in this study. Due to the chip geometry displayed in Fig. 1 there are four possible types of drop shape. They appear sequentially by the increase of flow rate of dispersed phase while keeping the flow rate of the continuous phase constant. A flow map depicting the occurrence of each shape is presented in Fig. 9.

At large enough flow rates of continuous phase $Q_c \geq 0.04$ mL/min and small enough flow rates of dispersed phase, spherical droplets are formed with diameter d < 190 μm. At the increase of the dispersed phase flow rate or the decrease of the continuous phase flow rate one still can see the circular 2D image, but the 3D shape becomes pancake-like. The pancake formation starts when the flow rate ratio exceeds certain threshold value φ_{d_p}, which increases with the flow rate of the continuous phase from $\varphi_{d\_p} = 0.15$ at $Q_c = 0.04$ to $\varphi_{d\_p} = 0.4$ at $Q_c = 0.1$ for the surfactant free system.

It is well known that for drop formation in unconfined geometry a decrease of the interfacial tension results in a decrease of drop size. The transition from the droplet to pancake region mostly follows this rule and is in line with discussion based on the dynamic surface tension. Transition for 0.35 mM of $C_{16}TAB$ occurs at the same flow rates as transition in surfactant-free system confirming equality of dynamic interfacial tension for this surfactant solution on the corresponding time scale (5–40 ms) and surfactant-free aqueous phase. For all other surfactant solutions smaller droplets are formed at the same conditions and therefore larger flow rate of dispersed phase is necessary for the droplet/pancake transition.

As expected from the analysis of dynamic surface tension, transition occurs at lower flow rate of dispersed phase for 5 mM solution of $C_{12}TAB$ than for both solutions having concentrations above *CMC*. Only at high flow rate does the performance of 5 mM $C_{12}TAB$ become close to that of 5 mM $C_{16}TAB$. The line for droplet/pancake transition for 50 mM $C_{12}TAB$ corresponds to the highest flow rates among all studied solutions up to flow rate of continuous phase 0.08 mL/min. But after that transition occurs at smaller flow rate ratios as compared to 5 mM $C_{12}TAB$ and 5 mM $C_{16}TAB$ solutions. This obvious discrepancy is due to change of dynamic regime. Transition from a droplet to pancake formation occurs in dripping regime for 5 mM $C_{12}TAB$ and 5 mM $C_{16}TAB$ solutions, whereas for 50 mM $C_{12}TAB$ it coincides with transition to jetting at the flow rate of continuous phase 0.06 mL/min and flow rate of dispersed phase 0.04 mL/min. This transition occurs at the same flow rate of dispersed phase by the increase of flow rate of continuous phase up to 0.1 mM/min. There are always droplets formed in dripping regime and pancakes formed in jetting regime, therefore transition from droplet to pancake remains at the same flow rate of dispersed phase at $Q_c \geq 0.06$ mL/min.

With further increase of flow rate of dispersed phase the diameter of the pancake increases until it reaches the value close to the channel width. After that the length of the drop along the channel axis becomes larger than that in perpendicular direction and a plug is formed. In distinction from droplet/pancake transition the critical flow rate ratio for transition to plug decreases rather slowly with the increase of the continuous phase flow rate, from 3 at $Q_c = 0.003$ to 1.4 at $Q_c = 0.07$ for surfactant-free system. At higher flow rates of continuous phase plugs were not observed in surfactant-free system. In surfactant-laden systems plugs were observed in the whole studied range of continuous phase flow rates.

Transition from pancake to plug occurs under the same conditions for solutions of 0.35 mM $C_{16}TAB$ and surfactant-free-aqueous phase. For surfactants demonstrating lower dynamic interfacial tension on the time scale of experiment this transition goes to lower flow rates of dispersed phase. For those solutions there is no clear dependence of transition on expected dynamic interfacial tension and this ambiguity is again the consequence of different dynamic regimes related to this transition. In particular, transition from pancake to plug can occur inside the dripping regime, inside the jetting regime or by transition from dripping to jetting.

Thus it can be concluded that transitions between various drop shapes occur smoothly and follow dynamic surface tension of corresponding solutions if they occur inside of the same dynamic regime. Switching regime can cause considerable jump in the size and therefore in the shape of drop formed by the dispersed phase.

The transition to threading was discussed in Fig. 5 above. The behaviour of surfactant solutions at this transition is in good agreement with estimated values of dynamic interfacial tension. This is clearly displayed by the lines sequence in the area 3 of Fig. 9. The threshold flow rate ratio for this transition decreases with the increase of continuous phase flow rate, but the decrease is rather slow. At $Q_c > 0.02$ mL/min threading was not observed for the studied range of the inner phase flow rates for surfactant-free system. For 50 and 150 mM solution of $C_{12}TAB$ the thread was observed at flow rates of continuous phase up to 0.05 mL/min.

The length of the formed drops (droplets, pancakes and plugs) along the channel axis increases with the increase of flow rate ratio according to power law $L \sim \varphi^{\alpha}$, but this increase is slow at small φ and becomes considerably faster after transition to plug formation (Fig. 10). The power law exponent, α_1, for droplets and pancakes formation both in dripping and squeezing mode is about 0.1, i.e. drop size increases slowly at this range of drop sizes and the increase in the flow rate of dispersed phase and corresponding increase in the flow rate ratio results mostly in the decrease of formation time per drop (Fig. 11). The jetting mode, where pancakes were formed, is excluded from this analysis because this transition resulted in a large jump in the pancakes size. Note, although the slope is nearly the same for different flow rates, the length values shift down with the increase of continuous phase flow rate. The transition to faster increase of the size with flow rate ratio occurs at $Q_d/Q_c \sim 1$ and is related to transition from the pancake to the plug structure.

For the plugs there is no systematic dependence of the size on the continuous phase flow rate and the power law exponent, α_2,

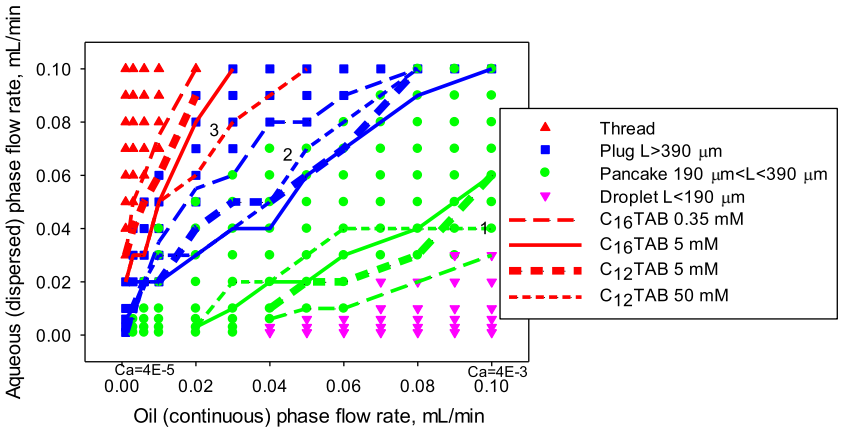

Fig. 9. Changes in flow map for the drop shape due to surfactant effect: symbols depict the structures formed in surfactant-free system; all large dashed lines correspond to C_{16}TAB 0.35 mM, all solid lines correspond to C_{16}TAB 5 mM, all dotted lines correspond to C_{12}TAB 0.35 mM, all short dashed lines correspond to C_{12}TAB 50 mM; green lines (area 1) show transition from a droplet to a pancake, blue lines (area 2) show transition from a pancake to a plug and red lines (area 3) show transition from a plug to a thread for corresponding surfactant solutions. (For interpretation of the references to colour in this figure legend, the reader is referred to the web version of this article.)

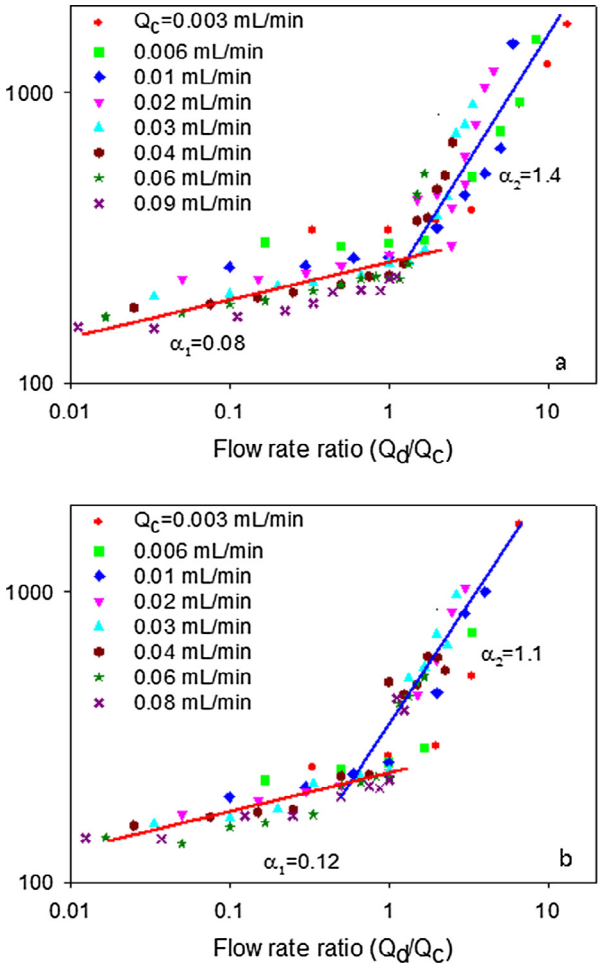

Fig. 10. Dependence of drop length of flow rate ratio for surfactant-free dispersed phase (a) and that containing 5 mM of C_{16}TAB (b).

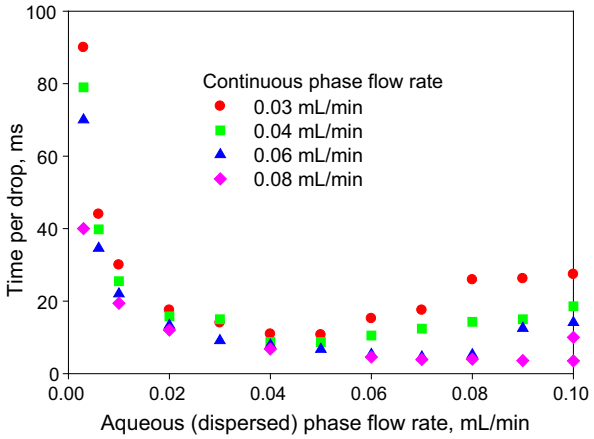

Fig. 11. Dependence of time per drop on flow rate of dispersed phase for surfactant-free system.

is about 1.4 for surfactant-free system and about 1 for surfactant-laden systems with dynamic interfacial tension different from that of surfactant-free solution (see Table 2). In general, addition of surfactant results in the slight increase of α_1 and decrease of α_2. The deviations from the power law for the plug structures presented in Fig. 10 have been observed only for C_{12}TAB 50 and 150 mM at flow rates of continuous phase $Q_c > 0.04$ mL/min. For these conditions transition from dripping to jetting resulted in formation of drops of pancake size, which were, however, considerably larger than drops formed in dripping mode. These drops grow faster than pancakes formed in dripping mode, but slower than plugs, being both pancake and plug size.

The difference in the power law exponent for plugs and droplets/pancakes is due to differences in the flow conditions. For the latter structures there is always possibility of bulk flow of continuous phase on the sides of channel, whereas for around the plug continuous phase remains only in thin liquid films between the channel walls and the plug.

Note, the plug formation is related to three distinct dynamic regimes: unstable jetting, drop coalescence at junction in dripping regime and plug formation in squeezing regime. However independently of regime, the formed plug obstructs the microchannel cross section. Therefore the rate of plug growth is determined mostly by geometrical restrictions independently of dynamic regime observed. That is why independently of dynamic regime the power law exponent for the plugs is close to 1, i.e. the plug length is proportional to the flow rate ratio, as predicted for squeezing regime in flow focusing device (Roche et al., 2009).

Table 2
Dependence of power law exponents (Fig. 10) on composition of dispersed phase.

Surfactant	No surfactant	C_{16}TAB, 0.35 mM	C_{16}TAB, 5 mM	C_{12}TAB, 5 mM	C_{12}TAB, 50 mM	C_{12}TAB, 150 mM
α1	0.08	0.08	0.12	0.09	0.10	0.08
α2	1.4	1.5	1.1	1.0	1.0	0.9

3.4. Drop coalescence

Despite the assumed stabilisation of the drops by the adsorbed surfactant, drop coalescence along the channel was observed for both C_{16}TAB and C_{12}TAB even at concentrations above CMC (see Fig. 12 and Table 3). For example for C_{16}TAB 5 mM at $Q_c = Q_d = 0.006$ mL/min only 17% of drops did not coalesce at a distance of 3 mm from junction, and for C_{12}TAB 50 mM at $Q_c = Q_d = 0.01$ mL/min 21% drops did not coalesce. Coalescence for C_{16}TAB occurred mostly at distance 1.6 ± 0.5 mm from the junction. Taking into account the time between drops (0.07 s for flow rates 0.006 mL/min) and data on dynamic surface tension (Fig. 3) it can be concluded that immediately after the drop formation the surface coverage is not yet complete. Thus, when the drop moved down the channel an additional amount of surfactant is still being adsorbed. From the drop velocity (4.5 mm/s) this additional time for adsorption can be estimated as 0.3 s. Therefore, at the point where the coalescence takes place, surface coverage can be still out of equilibrium and therefore the surfactant does not provide full "protection" against the coalescence. At the same time, the adsorption layer of C_{12}TAB 50 mM should already be at equilibrium on time scale of drop formation (0.05 s), see Fig. 3.

Noticeably, the percentage of coalescence for drops without surfactant is lower than that at high surfactant concentration at the same flow rate and nearly the same initial distance between drops: at $Q_c = 0.006$ and $Q_d = 0.01$ mL/min around 70% drops remain not coalesced for surfactant-free aqueous phase and only 21% for solution of 150 mM of C_{12}TAB.

Coalescence was observed for the pancakes and happened whenever two drops moved close to each other. In Fig. 13 the time dependence of the distance between drops at coalescence is shown for solution of C_{12}TAB at concentration 150 mM at $Q_c = Q_d = 0.01$ ml/min. Curves 1 and 2 represent two different pairs of coalescing drops. If the drops in the first pair are labelled as 1 and 2 then the next coalescing pair corresponds to drops 11 and 12. Curves 1 and 2 have different slopes, i.e. the approaching velocity for the coalescing drops varies over wide limits (see also data on standard deviations of the average velocity of approach in Table 3). Curves 3 and 4 show the surface to surface distance of the coalescing drops 11 and 12 to their nearest neighbours, 10 and 13. The time 0 for each pair corresponds to the pinch off moment of the second drop in the pair. The last point corresponds to the time when coalescence happens.

For each pair there is a decrease of the distance between the drops immediately after pinch off. This decrease is due to chip geometry presented in Fig. 1 (the increase in the cross-section between junction and the main channel). Pinch-off occurs in the junction and immediately after it the drop moves in the narrower part of channel with larger liquid velocity. Afterwards, the distance of coalescing drops to their closest neighbours changes very slowly, either decreasing or increasing. The coalescing drops approach each other more quickly and the movement accelerates before coalescence. This acceleration indicates the presence of an attraction force between drops which increases quickly with the decrease of distance. Indeed the hydrodynamic resistance to the motion of two non-deformable drops along the centre to centre line is inversely proportional to the distance between them (Cox, 1974), therefore the attraction force should increase faster than 1/h, where h is the surface to surface separation distance. There are always the random fluctuations in the distance between the drops. Some of these fluctuations can be amplified if even a small attractive force exists between the drops. Any repulsive force will stabilise the system.

For comparison curve 5 in Fig. 13 shows the approach kinetics for two surfactant-free drops. It shows that the approach is much slower than for surfactant-laden drops (See also Table 3) and there is no noticeable acceleration, on the contrary, drops stay quite close to each other for several milliseconds without coalescence.

It is seen from Fig. 12 that coalescence of surfactant-laden drops occurs inside 0.5 ms after the drop separation is still clearly distinguishable. This time is very small when compared to the literature data. According to (Gawel et al., 2015) the time between the visual contact of two millimetre size drops of crude oil in aqueous salts solution and the coalescence event was of the order of seconds for the drops stabilised by asphaltene and about 300 ms for the drops with extracted asphaltene. In Gawel et al. (2015)) experiments have been performed using two drops of equal size, which were slowly brought into contact using micro-translation stage. The volume of the surrounding aqueous phase was much larger than the drop volume, i.e. there was no geometrical restrictions imposed. The coalescence event was determined by the change of pressure inside the drops.

The lifetime of a soybean oil drop pressed by buoyancy to oil/water interface was studied in Basheva et al. (1999) in a wide range of drop sizes. Drops were stabilised by lyophilized bovine serum albumin dissolved in water. For the drops of radius around 100 μm the life time was on average several seconds.

In Krebs et al. (2013) coalescence of series of mineral and silicone oil drops in water (without any stabilising agent added) was studied in microfluidic device. The drops were formed in two T-junctions and brought from the opposite sides into a coalescence chamber having two side outlet channels. Due to small channels and chamber depths drops were also observed with the pancake shape. The hydraulic diameter of drops studied in Krebs et al. (2013)) was around 3 times smaller than that in our study. The coalescence time was defined in Krebs et al. (2013) as time between the moment when the surface to surface drop separation decreases to 1 μm and the moment of merging. This time was in the range of tens of milliseconds for all oils studied, what is still an order of magnitude higher than the one found in our study.

In Jose and Cubaud (2012) drops of water/glycerol mixture were produced in flow focusing device with silicone oil used as continuous phase. Coalescence was observed in diamond shape chamber with size 20 times larger than the channels. It was found that the coalescence time between the first contact of the drops and coalescence t_c was scaled by the viscous-capillary time scale t_{cap} as $t_c = 1000 t_{cap}$. According to (Jose and Cubaud, 2012) coalescence time for the system similar to that considered here should be in the range of tens of milliseconds.

Thus, the increase of the drops approach velocity and very short coalescence time both indicate some attraction force present in the system. To identify the possible force responsible for coalescence of surfactant-laden drops it should be taken into account that surfactants used in this study are ionic and the coalescing drops have

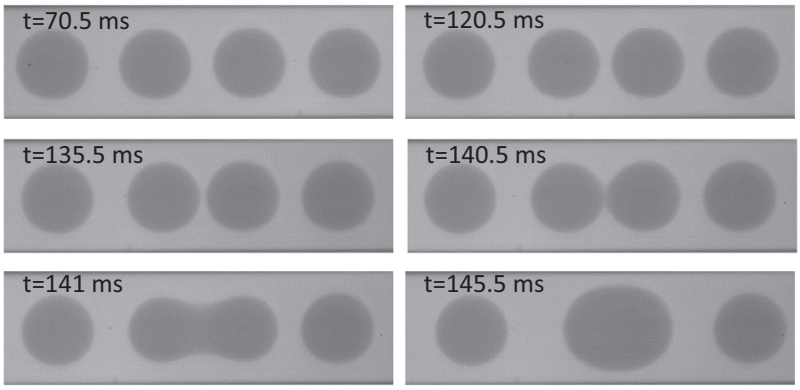

Fig. 12. Coalescence of drops stabilised by 150 mM C_{12}TAB. $Q_c = Q_d = 0.01$ mL/min.

Table 3
Parameters of drop coalescence in the microchannel.

Q_c/Q_d, ml/min	Surfactant	Average approach velocity, mm/s[a]	Non-coalesced,%	Initial distance between drops, μm[a]
0.006/ 0.01	No. Surfactant	0.19 ± 0.10	70	60 ± 2
0.006/ 0.01	C16TAB, 0.35 mM	0.33 ± 0.10	80	84 ± 1
0.006/ 0.006	C_{16}TAB, 5 mM	0.65 ± 0.25	17	122 ± 4
0.006/ 0.01	C_{16}TAB, 5 mM	1.18 ± 0.71	6	36 ± 3
0.006/ 0.01	C_{12}TAB, 5 mM	0.72 ± 0.33	49	51 ± 3
0.05/0.04	C_{12}TAB, 5 mM	2.42 ± 0.52	17	69 ± 3
0.01/0.01	C_{12}TAB, 50 mM	0.59 ± 0.14	21	101 ± 4
0.006/ 0.01	C_{12}TAB, 150 mM	0.98 ± 0.60	21	61 ± 6
0.01/0.01	C_{12}TAB, 150 mM	0.62 ± 0.16	75	118 ± 3

[a] Initial distance between the drops, h_i, is the surface to surface distance at the moment immediately after pinch-off of the second drop in the coalescing pair. This moment was defined as t_0. Coalescence time t_c is defined as a time when drops are visibly merged (t = 70.5 ms in Fig. 12). The average approach velocity $V_{av} = \frac{h_i}{t_c - t_0}$.

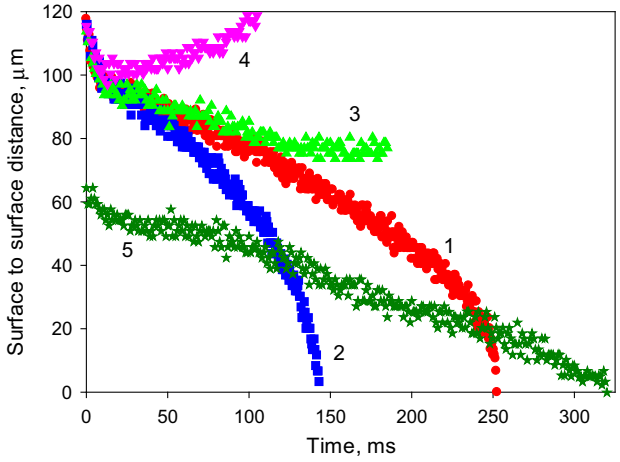

Fig. 13. Surface to surface distance between two arbitrary pairs of drops before coalescence: 1 – drops 1 and 2, 2 – drops 11 and 12, 3 – drops 12 and 13, 4 – drops 10 and 11 (aqueous phase contains 150 mM C_{12}TAB, $Q_c = Q_d = 0.01$ mL/min, L = 253 μm), 5 – system without surfactant ($Q_c = 0.006$ mL/min, $Q_d = 0.01$ mL/mim, L = 311 μm).

the pancake shape. The latter means that the drop surface is very close to the channel wall and therefore undergoes the essential shear stresses due to non-slip boundary conditions on the wall. The shear stress can produce a non-uniform surfactant distribution over the drop surface with depletion at the front and an increased surfactant concentration at the rear (Danov et al., 2003; Levich, 1962). Although each drop is electrically neutral, there is a surface charge as the counter-ions are distributed in the electrical double layer. When the interface moves due to shear stresses near the wall, convection transfers into the bulk, but the velocity of this movement decreases towards the channel axis, i.e. the counter-ions in the distant parts of the electric double-layer move slower than the surface active ions. This results in an excess of the surface active ions at the rear of the drop and the excess of the oppositely charged counter-ions at the front of the drop. Therefore there can be a charge disbalance inside the drop resulting in its polarisation and a dipole attraction between the drops.

Taking into account the large amount of parameters affecting drops interaction, namely drop size, distance between drops, drop velocity, surfactant concentration and adsorption kinetics it is impossible to make strict validation of the proposed mechanism with the experimental protocol used in this study, because all affecting parameters are interdependent. In the future, a more complicated geometry of microfluidic chip should be developed enabling independent variation at least some of these parameters to enable the phenomena to be elucidated separately.

4. Conclusions

Drop formation in flow-focusing microfluidic device occurs through one of three flow regimes: squeezing, dripping and jetting. In the fourth observed regime, threading, drops were not formed anymore. Squeezing is observed at small flow rates of continuous phase corresponding to capillary numbers $Ca_c < 0.001$ independent of the presence of surfactant. Dripping to jetting and jetting to threading transitions appear successively with the increase of flow rate of dispersed phase. Critical flow rate ratio for these transitions decreases with the increase of outer phase flow rate and, at given flow rate of continuous phase, decreases with surfactant addition.

The effect of surfactant depends on its concentration and value of critical micelle concentration and is in agreement with the values of dynamic surface tension measured on corresponding time-

scale. If concentrations of two surfactants normalised by CMC are similar then the effect of surfactant with larger value of CMC is stronger. If surfactants have the same molar concentration then the effect of surfactant with smaller CMC is stronger. Assuming that the value of capillary number of dispersed phase at transition from dripping to jetting is independent of surfactant presence, the dynamic interfacial tension can be calculated from the comparison the data for surfactant-free and surfactant-laden systems.

Drops formed in dripping mode (size smaller than the channel width) are much more uniform than those formed in squeezing and jetting modes. The size of formed drops increases with the increase of flow rate ratio. The power law exponent for the formation of drops with the size smaller than the width of channel is about 0.1, i.e. drop size increases slowly at this range of drop sizes and the increase of flow rate results mostly in the increase of time per drop. For plugs having the length larger than the width of channel the power law exponent is about 1.4 for surfactant-free system and about 1 for surfactant-laden systems.

The drops with size smaller than channel width, but larger than channel height (pancakes) coalesce while moving along the channel with coalescence rate being considerably higher for surfactant-laden drops. Analysis of video-recordings has shown that surfactant-laden drops approach each other much faster than surfactant-free ones and the approach velocity increases when surface to surface distance decreases. Such acceleration was not observed for surfactant-free drops. It is suggested that the coalescence of surfactant-laden drops is facilitated by the electrostatic dipole attraction due to non-uniform distribution of ionic surfactant over the drop surface. The non-uniform distribution is formed by high shear stresses near the wall.

Acknowledgements

This work is funded by the EPSRC Programme Grant "MEMPHIS – Multiscale Examination of Multiphase Physics in Flows" (EP/K003976/1).

References

Abate, A.R., Poitzsch, A., Hwang, Y., Lee, J., Czerwinska, J., Weitz, D.A., 2009. Impact of inlet channel geometry on microfluidic drop formation. Phys. Rev. E 80, 026310.
Anna, S.L., Bontoux, N., Stone, H.A., 2003. Formation of dispersions using flow focusing in microchannels. Appl. Phys. Lett. 82, 364–366.
Anna, S.L., Mayer, H.C., 2006. Microscale tipstreaming in a microfluidic flow focusing device. Phys. Fluids 18, 121512.
Anna, S.L., 2016. Droplets and bubbles in microfluidic devices. Annu. Rev. Fluid Mech. 48, 285–309.
Bai, L., Fu, Y., Zhao, S., Cheng, Y., 2016. Droplet formation in a microfluidic T-junction involving highly viscous fluid systems. Chem. Eng. Sci. 145, 141–148.
Bardin, D., Kendall, M.R., Dayton, P.A., Lee, A.P., 2013. Parallel generation of uniform fine droplets at hundreds of kilohertz in a flow-focusing module. Biomicrofluidics 7, 034112.
Baret, J.-C., Kleinschmidt, F., El Harrak, A., Griffits, A.D., 2009. Kinetic aspects of emulsion stabilization by surfactant: a microfluidic analysis. Langmuir 25, 6088–6093.
Baret, J.-C., 2012. Surfactants in droplet-based microfluidics. Lab Chip 12, 422–433.
Basheva, E.S., Gurkov, T.D., Ivanov, I.B., Bantchev, G.B., Campbell, B., Borwankar, R.P., 1999. Size dependence of the stability of emulsion drops pressed against a large interface. Langmuir 15, 6764–6769.
Bremond, N., Thiam, A.R., Bebette, J., 2008. Decompressing emulsion droplets favors coalescence. Phys. Rev. Lett. 100, 024501.
Brosseau, Q., Vrignon, J., Baret, J.C., 2014. Microfluidic dynamic interfacial tensiometry (μDIT). Soft Matter 10, 3066.
Chen, X., Glawdel, T., Cui, N., Ren, C.L., 2015. Model of droplet generation in flow focusing generators operating in the squeezing regime. Microfluid Nanofluid 18, 1341–1353.
Chen, Y., Liu, G.T., Xu, J.H., Luo, G.S., 2015. The dynamic mass transfer of surfactants upon droplet formation in coaxial microfluidic device. Chem. Eng. Sci. 132, 1–8.
Christopher, G.F., Anna, S.L., 2007. Microfluidic methods for generating continuous droplet streams. J. Phys. D 40, R319–R336.
Cox, R.G., 1974. The motion of suspended particles almost in contact. Int. J. Multiphase flow 1, 343–371.
Cubaud, T., Mason, T.G., 2008. Capillary threads and viscous droplets in square microchannels. Phys. Fluids 20, 053302.
Danov, K.D., Valkovska, D.S., Kralchevsky, P.A., 2003. Hydrodynamic instability and coalescence of trains of emulsion drops or gas bubbles moving through a narrow capillary. J. Coll. Int. Sci. 267, 243–258.
Garstecki, P., Stone, H.A., Whitesides, G.M., 2005. Mechanism for flow-rate controlled breakup in confined geometries: a route to monodisperse emulsions. Phys. Rev. Lett. 94, 164501.
Gawel, B., Lesaint, C., Bandyopadhyay, S., Oye, G., 2015. Role of physicochemical and interfacial properties on the binary coalescence of crude oil drops in synthetic produced water. Energy Fuels 29, 512–519.
Glawdel, T., Elbuken, C., Ren, C.L., 2012. Droplet formation in microfluidic T-junction generators operating in the transitional regime. I. Exp. Observations Phys. Rev E 85, 016322.
Glawdel, T., Ren, C.L., 2012. Droplet formation in microfluidic T-junction generators operating in the transitional regime. III. Dynamic surfactant effects. Phys. Rev E 86, 026308.
Guillot, P., Ajdari, A., Goyon, J., Joanicot, M., Colin, A., 2009. Droplets and jets in microfluidic devices. C. R. Chimie 12, 247–257.
Humphry, K.J., Ajdari, A., Fernandez-Nieves, A., Stone, H.A., Weitz, D.A., 2009. Suppression of instabilities in multiphase flow by geometric confinement. Phys. Rev. E 79, 056310.
Joos, P., Van Uffelen, M., 1995. Theory of growing drop technique for measuring dynamic interfacial tension. J. Coll. Int. Sci. 171, 297–305.
Joos, P., 1999. Dynamic Surface Phenomena. VSP, Utrecht, The Netherlands.
Jose, B.M., Cubaud, T., 2012. Droplet arrangement and coalescence in diverging/converging microchannels. Microfluid Nanofluid 12, 687–696.
Kovalchuk, N.M., Nowak, E., Simmons, M.J.H., 2016. Effect of soluble surfactants on the kinetics of thinning of liquid bridges during drop formation and on size of satellite droplets. Langmuir 32, 5069–5077.
Krebs, T., Schroen, C.G.P.H., Boom, R.M., 2013. Coalescence kinetics of oil in water emulsions studied with microfluidics. Fuel 106, 327–334.
Lee, W., Walker, L.M., Anna, S.L., 2009. Role of geometry and fluid properties in droplet and thread formation process in planar flow focusing. Phys. Fluids 21, 032103.
Levich, V.G., 1962. Physicochemical Hydrodynamics. Prentice-Hall, Egelwood cliffs.
Liu, H., Zhang, Y., 2011. Droplet formation in microfluidic cross-junctions. Phys Fluids 23, 082101.
Muijlwijk, K., Hinderink, E., Ershov, D., Berton-Carabin, C., Schroen, K., 2016. Interfacial tension measured at high expansion rates and within milliseconds using microfluidics. J. Coll. Int. Sci. 470, 71–79.
Nie, Z., Seo, M., Xu, S., Lewis, P., Mok, M., Kumacheva, E., Whitesides, G.M., Garstecki, P., Stone, H.A., 2008. Emulsification in a microfluidic flow-focusing device: effect of the viscosities of the liquids. Microfluid Nanofluid 5, 585–594.
Pompano, R.R., Liu, W., Du, W., Ismagilow, R.F., 2011. Spatially defined arrays of droplets in one, two and three dimensions. Annu. Rev. Anal. Chem. 4, 59–81.
Roche, M., Aytouna, M., Bonn, D., Kellay, H., 2009. Effect of surface tension variations on the pinch-off behaviour of small fluid drops in the presence of surfactants. Phys. Rev. Letters 103, 264501.
Rodriquez- Rodriquez, J., Sevilla, A., Martinez-Bazan, C., Gordillo, J.M., 2015. Generation of microbubbles with application to industry and medicine. Annu. Rev. Fluid Mech. 47, 405–429.
Romero, P.A., Abate, A.R., 2012. Flow focusing geometry generates droplets through a plug and squeeze mechanism. Lab Chip 12, 5130–5132.
Seemann, R., Brinkmann, M., Pfohl, T., Herminghaus, S., 2012. Droplet based microfluidics. Rep. Prog. Phys. 75, 016601.
Son, Y., Martys, N.S., Hagedorn, J.G., Migler, K.B., 2003. Suppression of capillary instability of a polymeric thread via parallel plate confinement. Macromolecules 36, 5825–5833.
Steegmans, M.J., Warmerdam, A., Schroen, K.G.P.H., Boom, R.M., 2009. Dynamic interfacial tension measurements with microfluidic Y-junction. Langmuir 25, 9751–9758.
Tan, J., Xu, J.H., Li, S.W., Luo, G.S., 2008. Drop dispenser in a cross-junction microfluidic device: scaling and mechanism of break up. Chem. Eng. J. 136, 306–311.
Ushikubo, F.Y., Oliveira, D.R.B., Michelon, M., Cunha, R.L., 2015. Designing food structure using microfluidics. Food Eng. Rev. 7, 393–416.
Utada, A.S., Fernandez-Nieves, A., Stone, H.A., Weitz, D.A., 2007. Dripping to jetting transitions in coflowing liquid streams. Phys. Rev. Lett. 99, 094502.
Utada, A.S., Fernandez-Nieves, A., Gordillo, J.M., Weitz, D.A., 2008. Absolute instability of a liquid jet in a coflowing stream. Phys. Rev. Lett. 100, 014502.
Van Loo, S., Stoukatch, S., Kraft, M., Gilet, T., 2016. Droplet formation by squeezing in a microfluidic cross-junction. Microfluid Nanofluid 20, 146.
Vladisavljevic, G.T., 2016. Recent advances in the production of controllable multiple emulsions using microfabricated devices. Particuology 24, 1–17.
Wang, K., Lu, Y.C., Xu, J.H., Luo, G.S., 2009. Determination of dynamic interfacial tension and its effect on droplet formation in the T-shaped microdispersion process. Langmuir 25, 2153–2158.
Wang, K., Zhang, L., Zhang, W., Luo, G., 2016. Mass transfer controlled dynamic interfacial tension in microfluidic emulsification process. Langmuir 32, 3174–3185.
Ward, T., Faivre, M., Stone, H.A., 2010. Drop production and tip-streaming phenomenon in a microfluidic flow-focusing device via an interfacial chemical reaction. Langmuir 26, 9233–9239.
Whitesides, G.M., 2006. The origins and the future of microfluidics. Nature 442, 368–373.

Wilke, C.R., Chang, P., 1955. Correlation of diffusion coefficients in dilute solution. AIChE J. 1, 264–270.
Zhang, M., Wang, W., Xie, R., Ju, X., Liu, Z., Jiang, L., Chen, Q., Chu, L., 2016. Controllable microfluidic strategies for fabricating microparticles using emulsions as templates. Particuology 24, 18–31.
Zhou, C., Yue, P., Feng, J.J., 2006. Formation of simple and compound drops in microfluidic device. Phys. Fluids 18, 092105.
Zhou, Q., Sun, Y., Yi, S., Wang, K., Luo, G., 2016. Investigation of droplet coalescence in nanoparticle suspensions by a microfluidic collision experiment. Soft Matter 12, 1674–1682.